Food Hydrocolloids 173 (2026) 112255

Contents lists available at ScienceDirect

Food Hydrocolloids

journal homepage: www.elsevier.com/locate/foodhyd

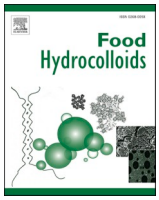

Curcumin distribution influences the properties of oil-water interfaces formed by kafirin nanoparticles

Ziyang Ye [a], Baohu Wu [b], Theresia Heiden-Hecht [b], Olaf Holderer [b], Leonard M.C. Sagis [a], Jasper Landman [a,*]

[a] Laboratory of Physics and Physical Chemistry of Foods, Wageningen University and Research, Bornse Weilanden 9, 6708WG, Wageningen, the Netherlands
[b] Jülich Centre for Neutron Science (JCNS) at Heinz Maier-Leibnitz Zentrum (MLZ), Forschungszentrum Jülich GmbH, Lichtenbergstr. 1, 85748, Garching, Germany

ARTICLE INFO

Keywords:
Kafirin nanoparticles
Bioactive distribution
Interfacial dilatational rheology
General stress decomposition
Pickering emulsion
Small-angle X-ray scattering

ABSTRACT

Kafirin nanoparticles (KNPs) are promising stabilizers for Pickering emulsions, but the influence of bio-actives on their oil-water interfacial properties remains unclear. This study aims to elucidate the influence of curcumin distribution, either encapsulated within particles or dissolved in the oil, on the interfacial behavior and emulsifying properties of KNPs. The general stress decomposition (GSD) method was employed to analyze whether the observed nonlinear behavior resulted from resistance to changes in network structure or surface density. Curcumin distribution markedly affected the interfacial behavior of KNPs: in both the linear and nonlinear regimes, curcumin-loaded kafirin nanoparticles (KCNPs) formed stiffer interfaces (E_d'≈11 mN/m) than KNPs (E_d'≈ 8 mN/m), while curcumin dissolved in the oil resulted in the weakest interface (E_d'<8 mN/m). We hypothesize that the oil phase has a partial plasticizing effect on the interfacial nanoparticle assembly, i.e., a partial relaxation of intermolecular constraints that softens the interfacial network. Curcumin encapsulation lessens this plasticizing effect by reducing particle-oil interactions. Indeed, small-angle X-ray scattering further reveals an increased alignment of the triglycerides in the oil phase with respect to the bulk, whereas KCNPs-stabilized emulsion shows reduced alignment, much closer to that of bulk oil. The resulting emulsion exhibited improved dynamic and storage stability compared with those stabilized by KNPs. The location of curcumin tunes interfacial properties and emulsion stability, providing mechanistic insight into designing protein-based Pickering delivery systems.

1. Introduction

Bioactive compounds are often hydrophobic, physically and chemically unstable within food systems, and exhibit limited bioavailability when used in their pure form (Alu'datt et al., 2022). Encapsulation is a widely used strategy to address these challenges (Liu et al., 2022; Nadendla et al., 2018). Curcumin has attracted attention as a model compound to improve bioavailability (Sabet et al., 2021). Several colloidal delivery systems have been explored, including protein-based nanoparticles, complexes, and emulsions (Abioye et al., 2024; Araiza-Calahorra et al., 2018; Ye et al., 2024). Among these systems, Pickering emulsions, stabilized by solid particles instead of surfactants, exhibit excellent physical stability and tunable interfacial properties, making them potential carriers for hydrophobic bio-actives like curcumin. In these emulsions, particles are typically irreversibly adsorbed at the oil-water interface and form kinetically stable emulsions, often exhibiting exceptional coalescence stability (Finkle et al., 1923), primarily due to the high attachment energy of particles at liquid-liquid interfaces (Binks & Lumsdon, 2001). To enhance the performance of Pickering emulsions for bioactive delivery, size, wettability, adsorption kinetics, shape and surface roughness of particles have been identified as key parameters influencing both emulsion droplet size and stability (Albert et al., 2019). With this in mind, and given the growing interest in more sustainable and food-compatible materials, plant protein-based nanoparticles have gained attention as potential alternatives to organic surfactants, thereby expanding the application of these particle-stabilized emulsions in pharmaceuticals and cosmetics (Destribats et al., 2014). In particular, prolamin-based nanoparticles have recently been studied for their oil-water interfacial and emulsion-stabilizing properties for the encapsulation of curcumin (Cui et al., 2024; Li et al., 2019, 2023; Wang et al., 2015; Wen et al., 2024; Zhou, Chen, et al., 2024).

Kafirin, the major storage protein of sorghum, is a prolamin rich in hydrophobic amino acids and disulfide bonds (Belton et al., 2006; Shah et al., 2021). Kafirin nanoparticles are typically compact and spherical,

* Corresponding author.
E-mail address: jasper.landman@wur.nl (J. Landman).

https://doi.org/10.1016/j.foodhyd.2025.112255
Received 22 August 2025; Received in revised form 6 November 2025; Accepted 13 November 2025
Available online 14 November 2025

with diameters ranging from 50 to 200 nm. Their highly hydrophobic surfaces facilitate their adsorption at oil-water interfaces (Xiao et al., 2015; Xiao et al., 2016). These nanoparticles have been employed to stabilize vegetable oil emulsions containing curcumin, and the resulting emulsions demonstrated good stability under acidic and refrigerated conditions (Xiao et al., 2015). In our previous work (Ye et al., 2024), curcumin was used as a model bioactive to develop curcumin-loaded kafirin nanoparticles with an average size of ~100 nm, which could be an interesting candidate to be used as a Pickering stabilizer. For effective stabilization, the particles should be at least 10–100 times smaller than the emulsion droplet size (Duffus et al., 2016). Sub-micron particles (~100 nm) are suitable for stabilizing droplets as small as a few micrometers (Chevalier & Bolzinger, 2013). This type of stabilization is achieved by adsorption of colloidal particles at the interface, which limits interfacial mobility and enhances the microstructural stability of emulsions (Hadidi et al., 2022; Jafari et al., 2020). There are still some knowledge gaps in kafirin nanoparticle-based Pickering stabilizers. On the one hand, curcumin-loaded kafirin nanoparticles have not been directly used as Pickering emulsifiers, and their oil-water interfacial properties are largely unknown. On the other hand, it remains unclear whether the incorporation of curcumin alters the interfacial behavior of the nanoparticles. Therefore, this study aims to investigate how curcumin localization—either within nanoparticles or in the oil phase—affects the interfacial behavior and emulsifying properties of kafirin nanoparticles.

We hypothesize that the localization of curcumin alters oil-particle interactions at the interface, which in turn affects particle-particle interactions, interfacial mechanical properties and emulsifying properties. In recent years, the nonlinear viscoelastic response regime in dilatational rheology has gained increased attention, as Lissajous plots provide direct insight into interfacial viscoelasticity and energy dissipation under large deformations, which are highly relevant to the processing and stability of food emulsions (Hashimoto et al., 2025; Ikenaga, de Groot, & Sagis, 2025; Ikenaga et al., 2025; Ikenaga & Sagis, 2024; Sagis & Yang, 2022). In our group we recently introduced the general stress decomposition method (GSD) (de Groot et al., 2023) which quantifies the nonlinear responses in dilatational rheology, and separates these responses into resistances to network deformations and changes in surface density. In addition, the structural organization of curcumin, nanoparticles and the oil phase can be analyzed using scattering techniques, such as Small-Angle X-ray Scattering (SAXS), which provide additional information on food systems over a wide range of length scales (Olakanmi et al., 2023), from the molecular scale up to the mesostructural scale. In nanoparticle research, SAXS not only allows characterization of particle shape—such as spheres, rods, disks, and ellipsoids—but also provides information on their arrangement at oil-water interfaces (Li et al., 2016; Tenorio-Garcia et al., 2024).

In this research, we systematically studied the effect of curcumin distribution on the oil-water interfacial behavior of kafirin nanoparticles and related these effects to their emulsifying properties. We determined the three-phase contact angle, interfacial adsorption behavior, and interfacial rheological properties in both the linear viscoelastic (LVE) and nonlinear viscoelastic (NLVE) regimes using an automated drop tensiometer (ADT). We used the general stress decomposition (GSD) method to quantify the nonlinear responses in dilatational rheology, and to relate these findings to changes in the interfacial network and resistance to changes in surface density of particle-stabilized interfaces. Finally, we prepared Pickering emulsions, characterized their droplet size distribution by light scattering, and observed oil-water interfaces using cryogenic scanning electron microscopy (Cryo-SEM). SAXS was used to investigate the interfacial characteristics and to establish a relationship between interfacial properties and emulsion stabilization mechanisms. Overall, this study will help to further understand and tailor the mechanical properties of kafirin nanoparticles through the incorporation of bioactive compounds, thereby enhancing their functionality and application in emulsion systems.

2. Materials and methods

2.1. Materials

Kafirin protein with a purity of 90 % was extracted and characterized using the method described in our previous work (Ye et al., 2024). Curcumin (CAS 458-37-7, ≥75 % HPLC, product no. 820354, Sigma-Aldrich, St. Louis, MO, USA) was used as received. All curcumin-containing samples were protected with aluminum foil from light during preparation and storage to prevent photodegradation. SAXS measurements were also conducted under dark conditions. Medium chain triacyl-glyceride (MCT) oil was purchased from a local market and purified before use to remove the surface-active impurities. Specifically, MCT oil was stripped by mixing with Florisil (100–200 mesh, magnesium silicate, Sigma-Aldrich, USA) overnight, followed by centrifuging twice at 2000× g for 20 min to remove residual Florisil. All other chemicals were of analytical grade or higher (Sigma-Aldrich, USA) and ultrapure water (MilliQ Purelab Ultra, Veolia, Germany) was used for all experiments.

2.2. Preparation of kafirin nanoparticles (KNPs) and curcumin-loaded kafirin nanoparticles (KCNPs)

Nanoparticles were prepared using an anti-solvent precipitation method with slight modifications compared to our previous research (Ye et al., 2024). A 3 % wt kafirin stock solution was prepared in 70 %, v/v ethanol solution. This stock solution was then mixed with a curcumin stock solution for 1 h while stirring at 600 rpm using a magnetic stirrer. These mixtures were then added dropwise into water to obtain KCNPs (with a kafirin mass fraction of 1 % wt, and a kafirin-to-curcumin mass ratio of 15:1), followed by continuous stirring at 600 rpm for another 30 min. KNPs were prepared based on the same method, but without the curcumin addition. The nanoparticle dispersions were dialyzed against distilled water (MWCO 3.5 kDa) to remove ethanol and centrifuged to collect the purified nanoparticles. The pH of the nanoparticle suspension was adjusted to 4 using a 1 M HCl solution. Finally, a portion of the particle suspension was stored, while the remainder was freeze-dried at a temperature of −80 °C under a vacuum pressure of 0.2 mbar for 48 h for later use. X-Ray diffraction (XRD) patterns were recorded on a Bruker D8-advance Diffractometer (Bruker AXS GmbH, Germany) with a copper target, voltage 40 kV, current 40 mA, and a scanning rate of 3° min^{-1}. The encapsulation efficiency was measured as 71 ± 3 %, which is consistent with our previous study (Ye et al., 2024).

2.3. Characteristics of nanoparticles

2.3.1. Particle size & zeta potential measurements

Particle size, polydispersity index (PDI), and zeta potential measurements were conducted using a freshly prepared dispersion of nanoparticles with a Zetasizer Ultra Nano ZS (Malvern Instruments, UK). Measurements were based on dynamic light scattering, which provided both electrophoretic mobility and particle size data. The refractive index of the medium was set to 1.33. All measurements were conducted at 20 °C in triplicate.

2.3.2. Three-phase contact angle measurement

The three phase contact angle was evaluated following the procedure of Wang et al. (2016) with slight modifications, using a droplet shape analyzer (DSA100, Krüss GmbH, Germany). Freeze-dried nanoparticles were compressed into pellets (2 mm thickness, 13 mm diameter). The pellet was then placed at the bottom of a cuvette containing MCT oil. Then, a 2 μL water droplet was carefully dripped onto the pellet surface with a high-precision syringe. The droplet was photographed immediately, and the contact angle θ was calculated by fitting the droplet profile to the Young−Laplace equation.

2.4. Adsorption behavior and interfacial dilatational rheology

The interfacial adsorption behavior and dilatational rheology of nanoparticles were determined using an automated drop tensiometer (TRACKER™, TECLIS Instruments, France), following the method of Yang et al. (2024) with some modifications. 0.5 % nanoparticle dispersion was added to the cuvette and controlled at 20 °C. A millimeter-sized droplet of MCT oil (with or without 0.06 % curcumin) with surface area of 30 mm^2 was formed at the tip of a G18 needle, submerged in the nanoparticle suspension. The density of the MCT oil and nanoparticle solution was set to 0.960 g/mL and 0.998 g/mL, respectively.

The interfacial adsorption behavior of the nanoparticles was investigated by measuring the change of interfacial pressure ($\Pi = \gamma_0$-γ_s) for 3 h, where γ_0 is the interfacial tension of the clean water-oil interface, and γ_s is the real-time interfacial tension of the sample. The interfacial tension was calculated by fitting the drop contour with the Young-Laplace equation for pendant drop analysis, as described by Berry et al. (2015).

After 3 h of equilibration, sinusoidal oscillatory deformations of the interface were applied using amplitude sweeps. In amplitude sweeps, the amplitude increased from 2 % to 50 % at a fixed frequency of 0.02 Hz with five cycles for each amplitude. This frequency was chosen to stay well below the upper limit of the drop tensiometer (~0.1 Hz) to ensure accurate sinusoidal deformations and avoid inertial effects at high deformation amplitudes. The data was used to calculate the first harmonic moduli (E_d' and E_d''). The values for these moduli are accurate only in the linear regime, since in the nonlinear regime the contributions from higher harmonics in the stress response are ignored. Therefore, in the nonlinear regime, the full surface stress signal, including contributions from higher harmonics, was further analyzed by constructing Lissajous plots (Sagis & Fischer, 2014), and further evaluated at large dilatational deformations using the general stress decomposition (GSD) method (de Groot et al., 2023), in which the Fourier transform of the stress response is split in separate contributions from odd and even harmonics. Measurements were performed at least three times at 20 °C.

In brief, the odd harmonics contain both an elastic part (τ_1) and a viscous part (τ_2), which describe the stress contributions due to interfacial network disruption. The even harmonics also consist of an elastic part (τ_4) and a viscous part (τ_3), which relate to the stress contributions due to interfacial density changes. These GSD components (τ_1-τ_4) can be quantified by several GSD parameters. For example, the slope of the τ_1 curve is represented by the secant modulus, $E_{\tau 1}$, which describes the contribution to interfacial stiffness from network interactions. The area of the closed loop of the τ_2 curve is equal to $U_{d\tau 2}$, which indicates the energy dissipation due to interfacial network disruption. The extent of the τ_4 curve is represented by a secant modulus, $E_{\tau 4}$, which describes the resistance of the interfaces in response to surface density changes. The viscous component of the even harmonics (τ_3) is quantified by $U_{d\tau 3}$, which equals the energy dissipation due to surface density changes. Those secant moduli and dissipation energies can be calculated using the following equations:

$$E_{\tau_1 L} = \frac{\sum_{k=0}^{i/2} b'_{2k+1}(-1)^k}{\varepsilon_0} \tag{1}$$

$$E_{\tau_4} = -\frac{\sum_{k=0}^{i/2} 2d'_{4k+2}}{\varepsilon_0} \tag{2}$$

$$U_{d\tau_2} = \pi \varepsilon_0^2 E''_d \tag{3}$$

$$U_{d\tau_3} = 2\varepsilon_0^2 \sum_{k=0}^{i/2} \frac{E_{2k\tau_3} * k}{k^2 - 1/4} \tag{4}$$

The coefficients b'_{2k+1} are the Fourier coefficients of τ_1, d'_{4k+2} are the Fourier coefficients of τ_4, $E''_d = b'_1/\varepsilon_0$, $E_{2k\tau_3} = c'_{2k}/\varepsilon_0$, c'_{2k} are the Fourier coefficients of τ_3, ε_0 is the amplitude of deformation, and i is the number of harmonics included in the analysis of the higher harmonics.

2.5. Preparation of pickering emulsions

MCT oil (with or without 0.06 % curcumin) was added dropwise into a 1 % wt nanoparticle dispersion while stirring with a high-speed mixer (T25 digital Ultra Turrax, IKA-Werke, Staufen, Germany) at 20,000 rpm, until reaching a final volume fraction of $\varphi = 20$ %. Mixing was continued for an additional 3 min after the oil addition was complete. The detailed calculation of the effective curcumin concentrations in these systems is provided in the supplementary materials (Sec. S1). This calculation shows that the effective concentrations of curcumin in droplets with 0.06 % in the oil phase, stabilized by KNPs, and those with curcumin in the nanoparticles (KCNPs), are roughly equal, and hence any differences in behavior of these two systems should be due to differences in localization of the curcumin.

2.6. Characteristics of emulsions stabilized by nanoparticles

2.6.1. Droplet size measurement

The droplet size distribution of freshly prepared emulsions was analyzed by light scattering using a Mastersizer 3000 (Malvern Panalytical, UK). For MCT oil, refractive and absorption indices of 1.45 and 0.001 were applied, respectively, while the dispersant refractive index was set to 1.33. The laser obscuration during measurements was maintained between 5 and 8 %.

2.6.2. Cryogenic scanning electron microscopy (Cryo-SEM)

The interfacial structure of emulsion droplets was probed using freeze-fracture scanning electron microscopy (Cryo-SEM). Each sample was placed on a Cu sample stub and immersed in liquid nitrogen. The frozen sample was then transferred under vacuum to a preparation chamber (ALTO 2500 Cryo Transfer System, UK) where it was fractured with a cooled knife. They were subjected to sublimation at −95 °C for 4 min to remove a controlled amount of water from emulsions, to expose their interfacial structure, and then sputter-coated with platinum. The sample was then transferred into a LEO 1530VP field emission scanning electron microscope with Oxford EDS detector for observation at −130 °C.

2.6.3. Dynamic stability

3 mL of freshly prepared emulsions were blended at 10,000 rpm for 1 min using a high-speed homogenizer (UltraTurrax, IKA, Staufen, Germany), followed by droplet size determination with the Mastersizer 3000.

2.6.4. Storage stability

Emulsions were stored at 4 °C for up to a month. The volume-based mean diameter ($D_{4,3}$) of the emulsions was measured over the storage period according to the procedure described in Sec. 2.6.1.

2.7. Small-angle X-ray scattering (SAXS)

SAXS is a useful tool for studying structure and interaction of complex systems, such as biomolecules, polymers, colloidal suspensions, and emulsions, with length scales ranging from nm to μm (Larson-Smith et al., 2010, 2012; Jeffries et al., 2021; Li et al., 2016). It enables direct detection of nanostructures and particle arrangement in emulsions in their dispersed state without removing the solvent. SAXS experiments were performed using a laboratory-based SAXS/WAXS/USAXS beamline KWS-X (XENOCS XEUSS 3.0 XL Garching Version) at JCNS MLZ, using a previously described method with minor modifications (Heiden-Hecht et al., 2024). The instrument was equipped with a D2+ Excillum Metal Jet X-ray source operating at 70 kV and 3.57 mA with Ga-Kα radiation (wavelength λ = 1.314 Å). Samples were measured in a glass capillary (2.0 mm ID) that was kept at ~25 °C. The sample-to-detector distances

were from 0.15 m to 1.70 m, which covered the scattering vector Q range from 0.004 to 3 $Å^{-1}$ ($Q = (4\pi/\lambda)\sin(\theta)$, 2θ is the scattering angle). The scattering patterns were obtained with a exposure time of 600 s and repeat to 6 times. The SAXS patterns were normalized to an absolute scale and azimuthally averaged to obtain the intensity profiles, and the solvent background was subtracted. The SAXS data were fitted with the Beaucage model (Beaucage, 1996). This model identifies the peaks and shoulders in the SAXS curves, which are linked to structural components within the sample.

2.8. Statistical analysis

Two-way analysis of variance (ANOVA) of the data was performed using R Studio software. A Tukey test was used for comparison of mean values among determinations at a significant level of 5 %. All experiments were conducted in triplicate. Data labeled with different lowercase letters are significantly different.

3. Results and discussions

3.1. Interfacial adsorption kinetics of nanoparticles at oil-water interfaces

As shown in Fig. 1A, both unloaded and curcumin-loaded nanoparticles exhibit a unimodal distribution with a peak at 50.79 nm, indicating the addition of curcumin does not affect the size and polydispersity. XRD analysis confirmed that no crystalline peaks of curcumin were observed in curcumin-loaded kafirin nanoparticles, whereas crystalline reflections of curcumin was still detected in the physical mixture of KNPs and curcumin (Fig. S1), which is consistent with the DSC findings in our previous study (Ye et al., 2024). This confirmed that curcumin was successfully entrapped in the particles.

The adsorption kinetics of these nanoparticles at oil-water interfaces was monitored using an automatic drop tensiometer as shown in Fig. 1C. Whether curcumin was encapsulated in the nanoparticles or dispersed in the oil phase, the nanoparticles absorbed at the interface at a similar rate, consistent with their similar size distributions and zeta-potentials (Fig. 1A and B). From 10 to 100s, the interfacial pressure increases rapidly, and after this initial phase, it reaches a plateau, with a similar interfacial pressure of ~12 mN/m for all three systems. The slow further increase in interfacial pressure is related to rearrangement at the interface through conformational changes and/or in-plane aggregation of nanoparticles at the interface (de Groot et al., 2024).

3.2. Interfacial dilatational rheology of nanoparticles at oil-water interfaces

To evaluate the mechanical properties of the oil-water interfaces stabilized by these nanoparticles, amplitude sweeps were conducted by applying amplitude deformations ranging from 2 % to 50 % at a fixed frequency of 0.02 Hz, a commonly used condition in interfacial rheology to ensure quasi-equilibrium responses. The resulting interfacial dilatational moduli are presented in Fig. 2. All interfaces exhibit a consistently higher storage modulus (E_d') than loss modulus (E_d''), concurrent with a tan $\delta' = E_d''/E_d'$ lower than 1, indicating these nanoparticles demonstrate elastic-dominated and solid-like behavior at oil-water interfaces (Kornet et al., 2022). The KNPs-stabilized interface shows a

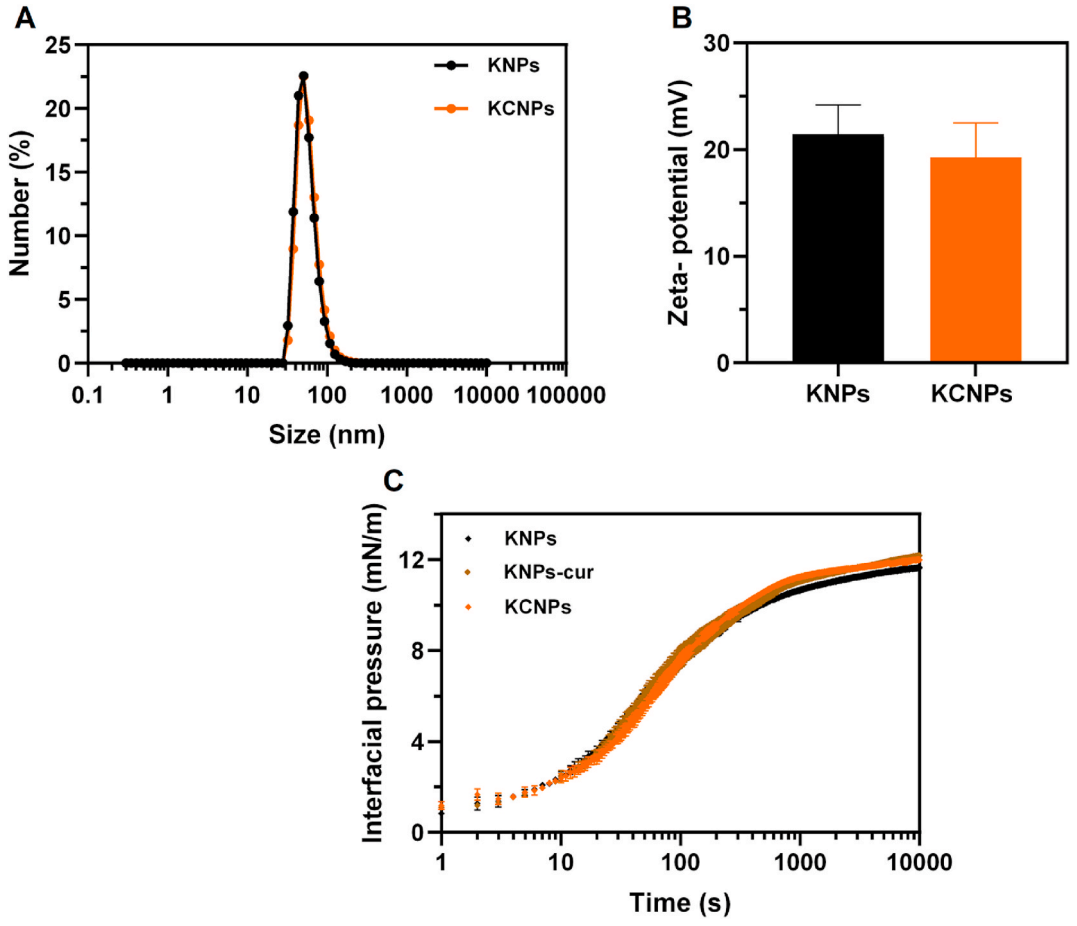

Fig. 1. Nanoparticle characteristics and adsorption behavior. Particle size distributions (A) and zeta-potential (B) of nanoparticle suspensions. Interfacial pressure (mN/m) as a function of time (s) (C) of kafirin nanoparticles (KNPs), KNPs with curcumin dispersed in MCT oil (KNPs-cur) and curcumin-loaded KNPs (KCNPs) at oil-water interfaces.

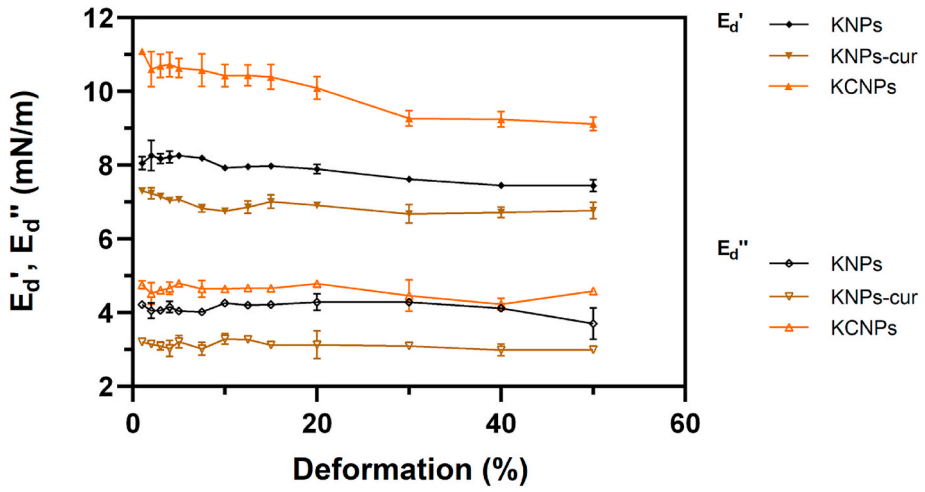

Fig. 2. Interfacial dilatational storage modulus (E_d') and loss modulus (E_d'') of the interfaces formed by kafirin nanoparticles (KNPs), KNPs with curcumin dispersed in MCT oil (KNPs-cur) and curcumin-loaded KNPs (KCNPs), as a function of deformation amplitude (%).

strain-independent E_d' of ~8 mN/m over the entire strain range, while the interface stabilized by KNPs-cur (KNPs with curcumin dispersed in MCT oil) has a slightly lower but also nearly constant E_d' of ~7 mN/m. When curcumin was encapsulated in the nanoparticles (KCNPs), E_d' remains approximately 11 mN/m within the linear viscoelastic regime (LVE) of the interface, up to ~15 % deformation. After that, the modulus decreases as the deformation increases because of the partial disruption of the interfacial structure or changes in interfacial density; however, at large deformations of 40 % and 50 %, the KCNPs-stabilized interface still retains a higher modulus compared to the other systems. Overall, KCNPs have stronger interactions among adjacent nanoparticles and form a stiffer oil-water interface compared to KNPs or KNPs-cur.

3.3. Lissajous plots

The calculation of Ed' in the large deformation regime was based on the first harmonic of the Fourier transform of the oscillatory interfacial stress, and the contributions from higher-order harmonics were neglected. To better understand the contributions of higher-order harmonics in the nonlinear regime of these nanoparticles at oil-water interfaces, Lissajous plots were constructed by plotting interfacial stress versus intracycle deformation (Ewoldt et al., 2008). During clockwise rotation from maximum negative to positive strain, the interface expands, followed by compression during the return to maximum negative strain. Consequently, the interfacial density varies throughout the cycle, and the dilatational plots show asymmetry with respect to the origin. Due to this asymmetry, the Fourier spectrum of the interfacial stress includes both odd and even harmonics (Bykov et al., 2015). A perfectly linear Lissajous plot represents a purely elastic interface, a circular plot signifies a purely viscous interface, and an elliptical plot indicates a viscoelastic interface (Ewoldt et al., 2008; Kamani et al., 2023).

In Fig. 3, all nanoparticles demonstrate narrow and near-elliptical

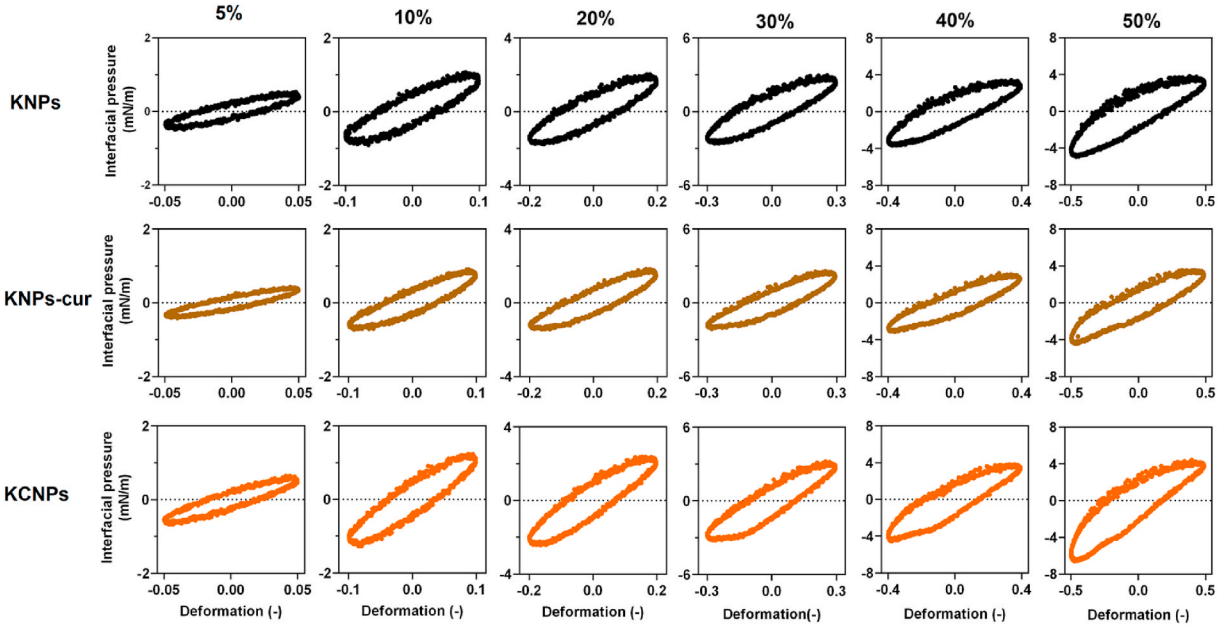

Fig. 3. Nonlinear dilatational rheology of nanoparticle-stabilized oil-water interfaces. Lissajous plots of interfacial pressure as a function of deformation amplitude for interfaces stabilized by kafirin nanoparticles (KNPs), KNPs with curcumin dispersed in MCT oil (KNPs-cur) and curcumin-loaded KNPs (KCNPs), at 5 %, 10 %, 20 %, 30 %, 40 % and 50 % deformation amplitudes at a fixed frequency of 0.02 Hz. For clarity, only one plot is shown for each amplitude, but all triplicate results are comparable.

shapes of Lissajous plots at a low deformation of 5 %, which indicates that the interfaces have predominantly elastic behavior. These plots become asymmetric with increasing deformations. The loops shown in KNPs-cur are narrower than those of other nanoparticles at each oscillation amplitude, suggesting a reduction in viscous dissipation and an enhancement of elastic behavior. Together with the lower dilatational modulus (Fig. 2), this indicates weaker interactions between the nanoparticles compared to the other two systems. At 20 % deformation and above, all systems show increasingly asymmetric plots. KCNPs demonstrate a relatively steep slope during the initial stages of expansion, but this slope decreases to almost zero towards maximum expansion. This points to strain softening, and hence a partial disruption of the interfacial microstructure. In the KNPs-cur-stabilized interface, this effect is less evident, which is in line with the almost constant values for E_d' in Fig. 2. In the compression phase, an almost straight line is observed for KNPs, which is indicative of a mild degree of strain hardening. The introduction of curcumin in both KNPs-cur and KCNPs leads to a different response during compression: the KCNPs-stabilized interface demonstrates obvious strain softening behavior towards maximum compression at 30 % deformation and higher, as evident from the fact that the interfacial pressure curve levels off to almost horizontal as maximum compression is approached. Interestingly, this softening behavior becomes less pronounced at 40 % and nearly disappears at 50 % deformation. This phenomenon also occurs in the KNPs-cur-stabilized interface, though it is less pronounced than in KCNPs. This strain softening can arise from several reasons, such as buckling of the interface or nanoparticles being expelled from the interface into the bulk phase. This will be further discussed in the next section.

3.4. General stress decomposition of Lissajous plots

To quantify the nonlinear behavior of the nanoparticle-stabilized interfaces, we used the general stress decomposition (GSD) method (de Groot et al., 2023) to decompose the Lissajous plots into odd and even harmonics, providing us with the four stress components τ_1, τ_2, τ_3 and τ_4. The odd harmonics, with their elastic and viscous components τ_1 and τ_2, reflect the contribution of network interactions to the interfacial stress. The viscous and elastic contributions of the even harmonics, given by τ_3 and τ_4, arise from density changes and are responsible for the asymmetry of the overall plots.

At 30 % deformation (Fig. 4), a narrow ellipsoidal plot is observed in the odd harmonics ($\tau_1+\tau_2$) of interfaces stabilized by KNPs and KNPs-cur, in which the plot of KNPs-cur is narrower, suggesting a predominantly elastic behavior without obvious network disruption. Notably, the interface stabilized by KCNPs shows a mild degree of strain softening behavior in compression and extension. KCNPs demonstrate a relatively steeper slope at 30–50 % deformation (Fig. S2, Fig. 4) compared to KNPs and KNPs-cur. This suggests that KCNPs maintain strong in-plane interactions even at large deformations.

To clarify this, the viscoelastic properties of the interfacial structures were quantified by several GSD parameters as shown in Fig. 5. $E_{\tau 1L}$ is the secant modulus of τ_1. In Fig. 5A, the interface stabilized by KNPs demonstrates almost constant $E_{\tau 1L}$ values of ~8 mN/m over the entire deformation amplitude range, slightly higher than the interface stabilized by KNPs-cur (~7 mN/m). The introduction of curcumin within the nanoparticles obviously alters the value of this modulus. KCNPs show $E_{\tau 1L}$ moduli ~11 mN/m at low strain amplitudes, which decrease with deformation, particularly at 20–30 % deformation. However, the value at 50 % deformation remains higher than that observed at other interfaces. This confirms that KCNPs have stronger in-plane interactions between the particles, resulting in stiffer interfacial structures that become increasingly disrupted as strain amplitude increases, consistent with previous findings (de Groot et al., 2023; Shen et al., 2025).

KCNPs-stabilized interface shows a very similar loop for τ_2 to KNPs at 40 % deformation, which is wider than the loop for KNPs-cur (Fig. S2). As the deformation increases to 50 %, KCNPs obviously demonstrate a

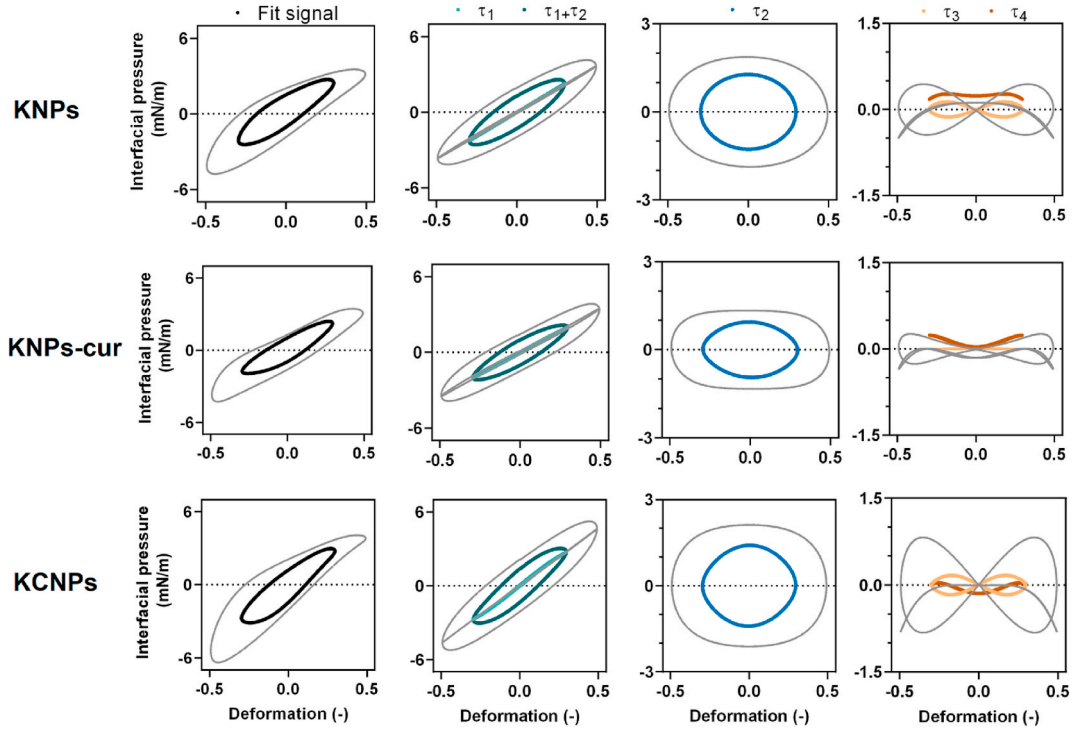

Fig. 4. General Stress Decomposition of Lissajous plots. The Lissajous plots at 30 % deformation amplitude were fitted and decomposed into curves of four stress components including τ_1, τ_2, τ_3 and τ_4 versus intra-cycle deformation for interfaces stabilized by kafirin nanoparticles (KNPs), KNPs with curcumin dispersed in MCT oil (KNPs-cur) and curcumin-loaded KNPs (KCNPs). The fitted plot is shown in black (—), τ_1 is shown in light green (—), $\tau_1+\tau_2$ is shown in dark green (—), τ_2 is shown in blue (—), τ_3 is shown in orange (—), and τ_4 is shown in brown (—). The corresponding components at 50 % deformation have been plotted in grey (—).

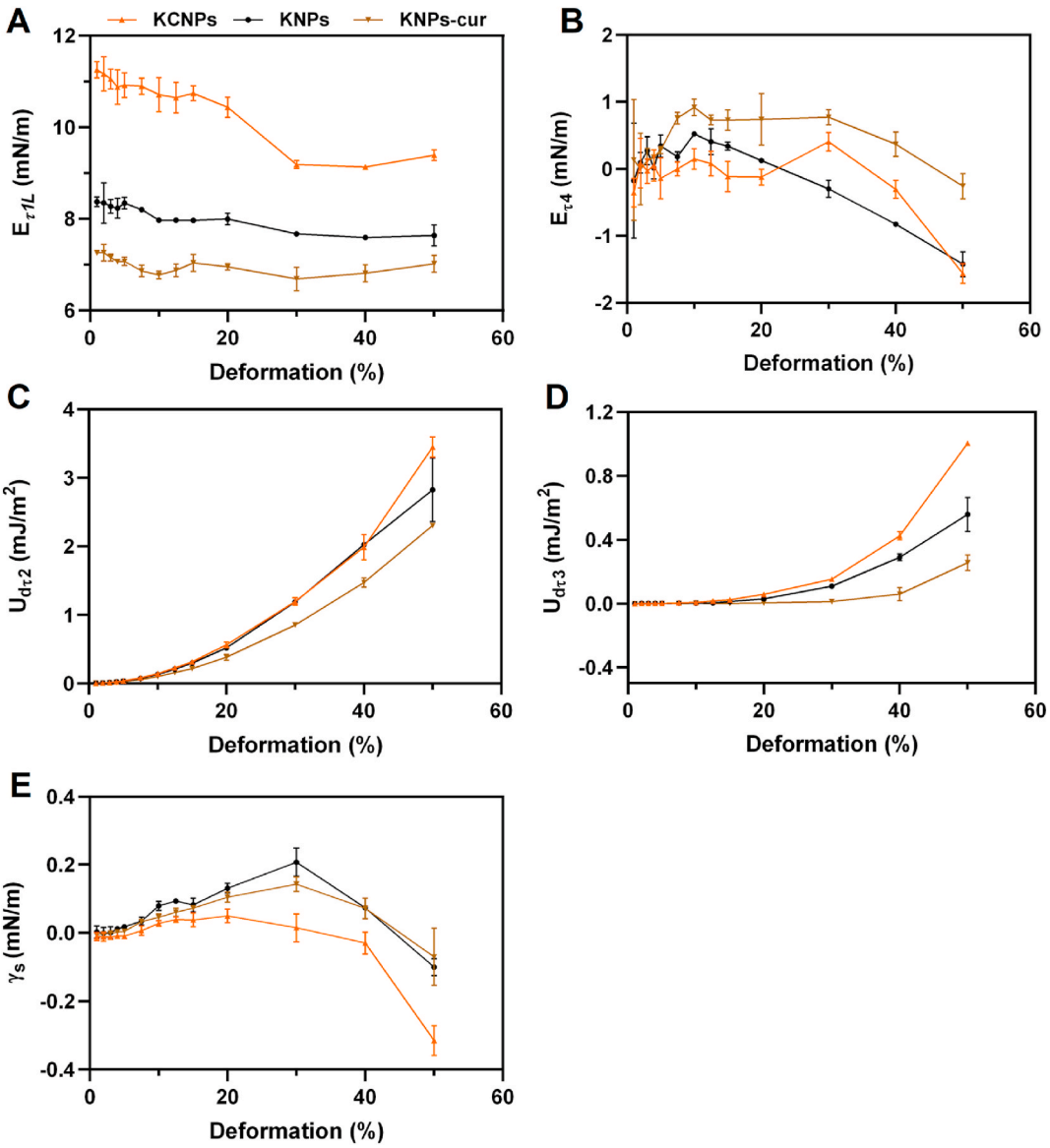

Fig. 5. Decomposed dilatational moduli of nanoparticle-stabilized oil-water interfaces. Modulus of τ_1 ($E_{\tau 1L}$) (A) and τ_4 ($E_{\tau 4}$) (B), dissipated energy of τ_2 ($U_{d\tau 2}$) (C) and τ_3 ($U_{d\tau 3}$) (D) and vertical shift (γ_s) (E) of interfaces stabilized by kafirin nanoparticles (KNPs), KNPs with curcumin dispersed in MCT oil (KNPs-cur) and curcumin-loaded KNPs (KCNPs), as a function of deformation amplitude after stress decomposition, performed at a fixed frequency of 0.02 Hz.

wider and more rectangular loop for τ_2 than KNPs, followed by KNPs-cur (Fig. 4). In Fig. 5C, this is quantified with the parameter $U_{d\tau 2}$, the dissipated energy per cycle for the odd harmonics. KNPs and KCNPs do not show any significant difference in $U_{d\tau 2}$ up to about 40 % deformation, but it is clearly higher at 50 % deformation for the KCNPs-stabilized interface, indicating a more significant partial disruption of the interfacial structures and an increase in viscous friction within the interface. In contrast, for the interface stabilized by KNPs-cur, $U_{d\tau 2}$ is clearly lower than that of the plain nanoparticles-stabilized interface as deformation increases.

The extent of the τ_4 curve is quantified by the secant modulus, $E_{\tau 4}$ (de Groot et al., 2023). Although the $E_{\tau 4}$ modulus of all systems is markedly smaller than $E_{\tau 1L}$, KCNPs exhibit generally more negative $E_{\tau 4}$ moduli than KNPs and KNPs-cur (Fig. 5B). This suggests increased contributions from surface density changes to the elastic response of these nanoparticle-stabilized interfaces. The baseline shift of τ_4 from the initial non-deformed state, γ_s, indicates that the interfaces are clearly driven out of equilibrium by the oscillations; KCNPs have the most negative value of γ_s (Fig. 5E), which indicates deformations around a dynamic state further from the interfacial equilibrium pressure-area isotherm. Apparently, due to slow in-plane relaxation, the KCNPs-stabilized interface cannot recover quickly enough to reach equilibrium at zero deformation.

The enclosed areas of the τ_3 curve represent the intra-cycle energy dissipation ($U_{d\tau 3}$) associated with the even harmonics. At 50 % deformation (Fig. 4), the introduction of curcumin within the nanoparticles again significantly increases this dissipated energy associated with density changes compared to KNPs. KNPs-cur again give the lowest values and are nearly 0 mJ/m^2 for almost the entire strain range. From both Fig. 5B and D, it is evident that KCNPs have the highest $U_{d\tau 3}$ and most negative $E_{\tau 4}$ values, especially at 50 % deformation, while KNPs-cur display lower values than KNPs. This indicates that KCNPs form a more densely packed oil-water interface, with greater dissipation energy driven by surface density changes.

Overall, in the non-linear viscoelastic (NLVE) regime, $E_{\tau 1L}$ and $U_{d\tau 2}$ are significantly larger than $E_{\tau 4L}$ and $U_{d\tau 3}$ for all interfaces formed by nanoparticles, suggesting contributions of interfacial network changes dominate the nonlinear behavior of these nanoparticles at oil-water

interfaces. KCNPs have the highest $E_{\tau 1L}$ value and $U_{d\tau 2}$ even in this regime, suggesting the formation of stiffest interface with strongest in-plane interactions that dissipated most energy due to network disruption. The KCNPs-stabilized interface displays higher negative $E_{\tau 4}$ and γ_s values, which may indicate the formation of denser interface that is more resistant to surface density changes. All implies the encapsulation of curcumin in the nanoparticles has a significant effect on the interfacial properties of the oil-water interface, and results in a denser and stiffer structure. In contrast, curcumin dispersed in the oil phase demonstrates an opposite effect.

The contact angle of KNPs at the O/W interface is 108.6 ± 2.3°, as previously reported (Ye et al., 2025), indicating that KNPs tend to reside predominantly in the oil phase and interact strongly with it. The oil molecules can act as a plasticizer (Bergfreund et al., 2021; Ye et al., 2025). This leads to weaker in-plane interactions among the particles and results in the formation of a weaker interface, compared to the film they form at air-water interfaces. When curcumin was encapsulated in the nanoparticles, the surface hydrophobicity slightly decreases, and the contact angle decreases to 100.55 ± 0.86° (Fig. S3). A possible mechanism is that the curcumin binds to some of the hydrophobic sites of kafirin, thereby reducing the exposed hydrophobicity of the nanoparticles. With some of the hydrophobic sites blocked, the plasticizing effect of the oil molecules is likely reduced. As a result, the particles can form stronger in-plane particle-particle interactions, leading to a stiffer interface. This behavior is in line with the work of Zhou, Xin, et al. (2024), who reported that curcumin-zein complex demonstrated a slight decrease in oil-in-water contact angle compared to unloaded zein nanoparticles. In contrast, when curcumin was directly dispersed in the oil phase, the in-plane interactions between kafirin nanoparticles became weaker, which led to the formation of a weaker interface. This could be because curcumin exhibits minor adsorption at the interface (Fig. S4), which affects the ability of the particles to attach to the interface. This may affect the emulsifying properties of these nanoparticles, which will be further investigated in the next section.

3.5. Pickering emulsions stabilized by nanoparticles

Pickering emulsions stabilized by these nanoparticles were fabricated, and their droplet size distributions are shown in Fig. 6 (D-F). All three Pickering emulsions demonstrate a single peak at ~20 μm, suggesting that the addition of the curcumin, either inside the nanoparticles or in the oil phase, does not obviously affect the droplet size

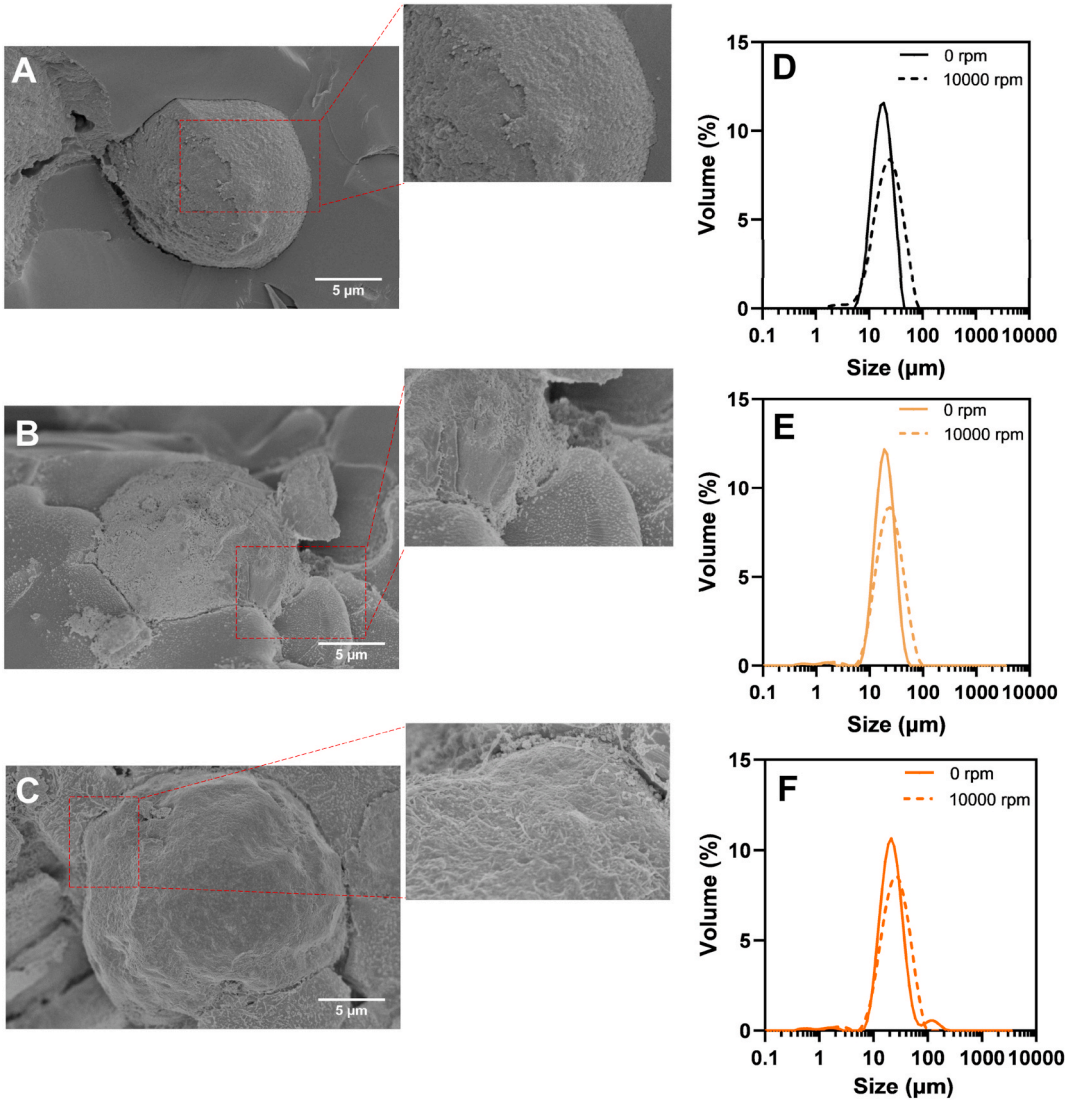

Fig. 6. Morphology of nanoparticle-stabilized emulsions. Cryo-SEM images of Pickering emulsions stabilized with kafirin nanoparticles (KNPs) (A), KNPs with curcumin dispersed in MCT oil (KNPs-cur) (B), and curcumin-loaded KNPs (KCNPs) (C). Droplet size distributions of the corresponding emulsions prepared with these nanoparticles before and after blending treatment at homogenization speed of 10,000 rpm (D–F).

distributions. The observed droplet size is smaller than that reported previously (Xiao et al., 2016), which may be attributed to differences in oil type (MCT compared with plant oils) and other preparation parameters (Tsabet & Fradette, 2015). To evaluate dynamic stability, these emulsions were subjected to a high-speed blender at 10000 rpm—lower than the speed used during preparation—and the volume-based droplet size distributions reflect their resistance to flow-induced changes. The emulsion stability was indicated by the volume percentage of the new peaks which appeared in the droplet size distributions. After treatment, all emulsions exhibit an increase in droplet size, in which KCNPs-stabilized emulsion showing the smallest volume change (13.74 %), suggesting better dynamic stability compared to KNPs (23.4 %) and KNPs-cur (20.01 %).

Cryo-SEM was used to visualize the oil-water interfaces of individual droplets, as shown in Fig. 6 (A-C). The surface of the oil droplets is covered by nanoparticles, confirming the formation of oil-water Pickering emulsions. Nanoparticles are observed on the droplet surface, as indicated in the zoomed-in images, providing structural basis for their resistance to coalescence during blending treatment and storage. Xiao et al. also used this technique to observe the interfacial structure formed by kafirin nanoparticles. Their results showed that kafirin particles anchor at the droplet surfaces (Xiao et al., 2016), which is consistent with our observations. The storage stability of these nanoparticles-stabilized emulsions was determined by droplet size measurement. In Fig. S5, the mean droplet size ($D_{4,3}$) increased in all emulsions after 7 days of storage, but remained stable thereafter until the end of the storage period. Among them, the KCNPs-stabilized emulsion demonstrates less variation in droplet size compared to the other systems throughout the entire storage period.

3.6. SAXS

In order to better understand the stabilization mechanisms of these emulsions, we conducted SAXS measurements on both the nanoparticles dispersions and the corresponding nanoparticle-stabilized emulsions. In SAXS curves, a high Q-value represents small structures, whereas a low Q-value corresponds to large structures. The size D of each feature, such as a peak or shoulder, can be estimated using equation $D = 2\pi/Q_{max}$. Both scattering data in Fig. 7A exhibit characteristic nanoparticle scattering behavior, $I \sim Q^{-4}$. The KNPs dispersion displays a smooth monotonic decay consistent with polydisperse particle distributions, where the signal clearly plateaus in the low-Q region. In contrast, the KCNPs profile maintains a finite slope at the minimal detectable Q-range, indicating minor populations of larger aggregates. Although KCNPs appear more prone to aggregation than KNPs, this was not resolved by DLS measurements (Fig. 1A). These datasets were fitted to a single level Beaucage model (Beaucage, 1996), implemented in SasView 5 (https://www.sasview.org). Fitted radius of gyration (R_g) values were comparable between the nanoparticles, with KNPs exhibiting an R_g of 19.4 nm and KCNPs of 20.3 nm (fits shown in Fig. S6). To elucidate particle morphology, a prolate ellipsoid model with polydispersity (~0.5) was also fitted to the data. The fits suggest both particle types to have polar-to-equatorial axial ratios of 2–3, suggesting both nanoparticle types adopt similar prolate ellipsoidal morphologies. The high polydispersity makes it difficult to obtain precise structural parameters; thus, the fits to the ellipsoidal model are interpreted as indicative only.

The emulsion scattering profiles (Fig. 7B) were fitted to a two-level Beaucage model. The R_g associated with Level 1 (emulsion droplet dimensions) exceeds the measurable Q-range, while Level 2 corresponds to nanoparticles, similar to the scattering patterns of the particle dispersions without oil. In general, the scattering patterns of the two emulsion types are very similar. Level 2 R_g values decrease slightly relative to dispersions—9.7 nm for KNPs-stabilized and 10.5 nm for KCNPs-stabilized emulsions—suggesting interfacial particle reorganization. For the low-Q regime, the power-law decay reflects the interface smoothness: a power law decay of −2 indicates that the particles form a perfectly flat interface, whereas exponents larger than 2 indicate increasing surface roughness. The power law decay exponents (the level 1 power law at small Q) are 2.54 for the emulsion stabilized with KNPs and 2.65 for that stabilized with KCNPs, suggesting that both interfaces are somewhat rough, with KCNPs forming a slightly rougher interface than KNPs. This SAXS interpretation is consistent with the Cryo-SEM observations (Fig. 6C), which also show more heterogeneous particle packing at KCNPs-stabilized interfaces.

All emulsions show a distinct high-Q peak (Fig. 8A) attributed to molecular ordering of medium-chain triglyceride (MCT) fatty acid chains. The peak intensity follows the order: KNPs-stabilized emulsion > KCNPs-stabilized emulsion > pure MCT oil. This demonstrates that KNPs induce substantial local alignment of MCT molecules. Conversely, the rougher interfaces formed by KCNPs and their reduced oil affinity disrupt this local ordering and produce scattering patterns that more closely resemble those of bulk MCT oil. To further explore this, we compared the scattering of MCT oil with and without curcumin dissolved in it (Fig. S7). The results showed changes only in the low-Q range, not in the high-Q range, confirming that the differences in oil ordering are not caused by curcumin dissolution in the oil. Therefore, they must result from the interaction between the MCT oil and the nanoparticles.

The schematic alignment of triglycerides is illustrated in Fig. 8B-D. When KNPs are used as an emulsifier, they exhibit strong interactions with MCT molecules, causing a measurable local alignment of MCT molecules. These interactions lead to weaker interactions between the particles themselves, resulting in the formation of a weaker oil-water interface and a less stable emulsion. KCNPs evidently interact less with MCT molecules, and consequently KCNPs can sustain stronger in-plane particle-particle interactions and form a stiffer and more densely

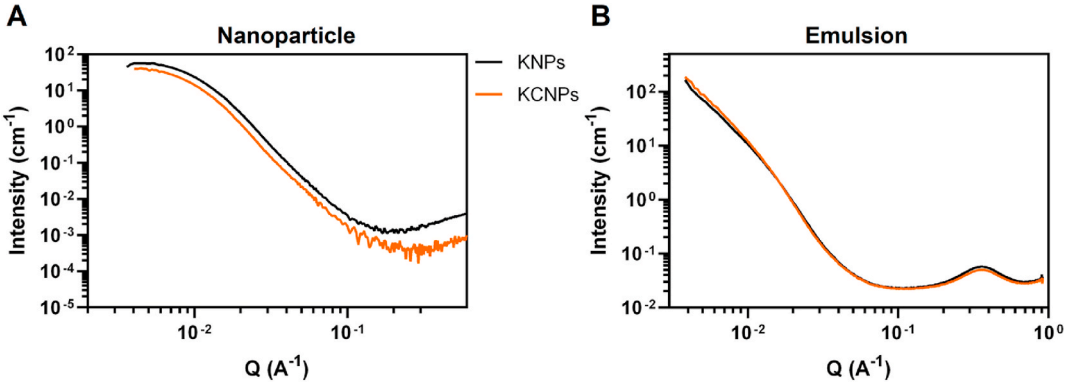

Fig. 7. Small-angle X-ray scattering (SAXS) patterns of (A) kafirin nanoparticles (KNPs) and curcumin-loaded KNPs (KCNPs), and (B) emulsions stabilized by these nanoparticles.

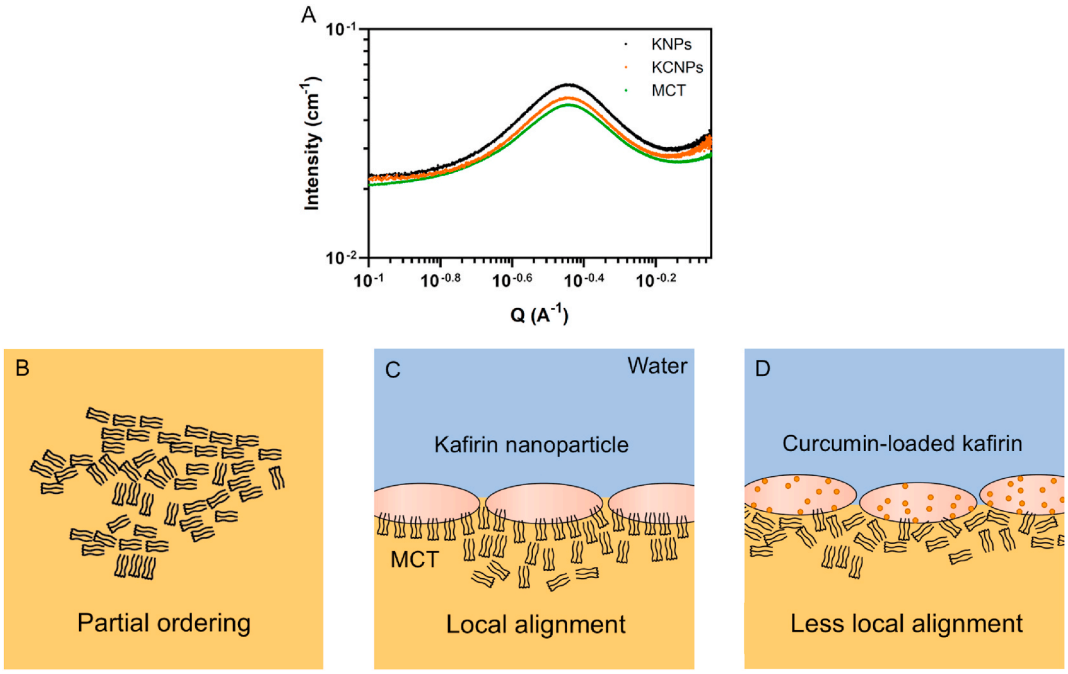

Fig. 8. Kafirin nanoparticles (KNPs) and curcumin-loaded KNPs (KCNPs) cause partial alignment of triglycerides. High Q-region small-angle X-ray scattering patterns of medium-chain triglycerides (MCT) and emulsions stabilized by KNPs and KCNPs, showing the alignment of the fatty acid chains. The scattering pattern of bulk MCT oil was rescaled to match the oil fraction (20 wt%) in the emulsions (A). Schematic illustrations of alignment of triglycerides in bulk MCT oil (B), in the vicinity of a KNPs-stabilized interface (C), and in the vicinity of a KCNPs-stabilized interface (D).

packed oil-water interface, which contributes to the improved dynamic and storage stability of the emulsion. These possible mechanisms highlight the connection between the interfacial properties of these nanoparticles and their emulsifying behavior.

Our experiments used water-insoluble curcumin as a model bioactive compound, and the findings can also be extended to other bioactives, such as β-carotene and various polyphenols. Because kafirin is structurally similar to zein and exhibits comparable self-assembly behavior, the insights obtained here are also relevant to other prolamin nanoparticles. Therefore, our results provide a theoretical basis for designing protein-based delivery systems beyond kafirin alone. In addition, formulation parameters such as particle size, surface hydrophobicity and bioactive loading of nanoparticles can be tailored to modulate interfacial properties, which in turn may enhance emulsion stability and help preserve sensitive bioactives in food and pharmaceutical systems.

4. Conclusions

In this study, we investigated the effect of curcumin distribution on the oil-water interface formed by kafirin nanoparticles using interfacial dilatational rheology. We aimed to understand how these particles adsorb at interfaces and respond to small and large deformations. Curcumin encapsulation had minimal influence on the particle size distribution and zeta-potential, resulting in a negligible effect on the interfacial adsorption behavior. However, the distribution of curcumin markedly influenced particle-particle interactions at interfaces, which affects the nonlinear behavior. Contributions from interfacial network interactions play a more dominant role in the nonlinear behavior of all three types of nanoparticles-stabilized interfaces, compared with surface density changes. Curcumin encapsulated in the nanoparticles improved interfacial stiffness, likely due to the formation of a more densely packed interface that is more resistant to network and density changes. This, in turn, enhanced the dynamic and storage stability of the corresponding emulsion. In contrast, curcumin dispersed in the oil phase led to a weaker interface than that formed by kafirin nanoparticles. These differences in curcumin distribution also altered the local ordering of the MCT molecules and affected the degree to which MCT molecules plasticize the particle network, further influencing the interfacial and emulsifying properties of these nanoparticles. Overall, these findings provide useful information on the effect of bioactives on the interfacial behavior of nanoparticles and contribute to the development of functional Pickering emulsions. Future studies could explore how these interfacial differences influence curcumin bioaccessibility during digestion.

CRediT authorship contribution statement

Ziyang Ye: Writing – review & editing, Writing – original draft, Visualization, Validation, Methodology, Investigation, Conceptualization. **Baohu Wu:** Investigation (SAXS experiments), Writing – review & editing. **Theresia Heiden-Hecht:** Writing – review & editing. **Olaf Holderer:** Formal analysis (SAXS data modeling), Writing – review & editing. **Leonard M.C. Sagis:** Writing – review & editing, Supervision, Methodology, Conceptualization. **Jasper Landman:** Writing – review & editing, Supervision, Methodology, Conceptualization.

Declaration of competing interest

The authors declared that no competing interests exist.

Acknowledgements

The authors would like to thank the Chinese Scholarship Council (CSC) for financial support. We also appreciate the assistance of Esther Blommert with Cryo-SEM visualization.

Appendix A. Supplementary data

Supplementary data to this article can be found online at https://doi.org/10.1016/j.foodhyd.2025.112255.

Data availability

Data will be made available on request.

References

Abioye, R. O., Obeme-Nmom, J. I., & Udenigwe, C. C. (2024). Pea protein–curcumin interactions and their effects on in vitro protein digestibility. *ACS Food Science & Technology, 4*(3), 711–718.

Albert, C., Beladjine, M., Tsapis, N., Fattal, E., Agnely, F., & Huang, N. (2019). Pickering emulsions: Preparation processes, key parameters governing their properties and potential for pharmaceutical applications. *Journal of Controlled Release, 309*, 302–332.

Alu'datt, M. H., Alrosan, M., Gammoh, S., Tranchant, C. C., Alhamad, M. N., Rababah, T., Zghoul, R.a., Alzoubi, H., Ghatasheh, S., & Ghozlan, K. (2022). Encapsulation-based technologies for bioactive compounds and their application in the food industry: A roadmap for food-derived functional and health-promoting ingredients. *Food Bioscience, 50*, Article 101971.

Araiza-Calahorra, A., Akhtar, M., & Sarkar, A. (2018). Recent advances in emulsion-based delivery approaches for curcumin: From encapsulation to bioaccessibility. *Trends in Food Science & Technology, 71*, 155–169.

Beaucage, G. (1996). Small-angle scattering from polymeric mass fractals of arbitrary mass-fractal dimension. *Journal of Applied Crystallography, 29*(2), 134–146.

Belton, P. S., Delgadillo, I., Halford, N. G., & Shewry, P. R. (2006). Kafirin structure and functionality. *Journal of Cereal Science, 44*(3), 272–286.

Bergfreund, J., Bertsch, P., & Fischer, P. (2021). Effect of the hydrophobic phase on interfacial phenomena of surfactants, proteins, and particles at fluid interfaces. *Current Opinion in Colloid & Interface Science, 56*, Article 101509.

Berry, J. D., Neeson, M. J., Dagastine, R. R., Chan, D. Y., & Tabor, R. F. (2015). Measurement of surface and interfacial tension using pendant drop tensiometry. *Journal of colloid and interface science, 454*, 226–237.

Binks, B. P., & Lumsdon, S. O. (2001). Pickering emulsions stabilized by monodisperse latex particles: Effects of particle size. *Langmuir, 17*(15), 4540–4547.

Bykov, A. G., Liggieri, L., Noskov, B. A., Pandolfini, P., Ravera, F., & Loglio, G. (2015). Surface dilational rheological properties in the nonlinear domain. *Advances in Colloid and Interface Science, 222*, 110–118.

Chevalier, Y., & Bolzinger, M.-A. (2013). Emulsions stabilized with solid nanoparticles: Pickering emulsions. *Colloids and Surfaces A: Physicochemical and Engineering Aspects, 439*, 23–34.

Cui, S., McClements, D. J., He, X., Xu, X., Tan, F., Yang, D., Sun, Q., & Dai, L. (2024). Interfacial properties and structure of pickering emulsions co-stabilized by different charge emulsifiers and zein nanoparticles. *Food Hydrocolloids, 146*, Article 109285.

de Groot, A., Sagis, L. M. C., & Yang, J. (2024). White asparagus stem proteins, from waste to interface stabilizer in food foams. *Food Hydrocolloids, 146*, Article 109218.

de Groot, A., Yang, J., & Sagis, L. M. C. (2023). Surface stress decomposition in large amplitude oscillatory interfacial dilatation of complex interfaces. *Journal of Colloid and Interface Science, 638*, 569–581.

Destribats, M., Gineste, S., Laurichesse, E., Tanner, H., Leal-Calderon, F., Heroguez, V., & Schmitt, V. (2014). Pickering emulsions: What are the main parameters determining the emulsion type and interfacial properties? *Langmuir, 30*(31), 9313–9326.

Duffus, L. J., Norton, J. E., Smith, P., Norton, I. T., & Spyropoulos, F. (2016). A comparative study on the capacity of a range of food-grade particles to form stable O/W and W/O pickering emulsions. *Journal of Colloid and Interface Science, 473*, 9–21.

Ewoldt, R. H., Hosoi, A. E., & McKinley, G. H. (2008). New measures for characterizing nonlinear viscoelasticity in large amplitude oscillatory shear. *Journal of Rheology, 52*(6), 1427–1458.

Finkle, P., Draper, H. D., & Hildebrand, J. H. (1923). THE THEORY OF EMULSIFICATION [1]. *Journal of the American Chemical Society, 45*(12), 2780–2788.

Hadidi, M., Boostani, S., & Jafari, S. M. (2022). Pea proteins as emerging biopolymers for the emulsification and encapsulation of food bioactives. *Food Hydrocolloids, 126*, Article 107474.

Hashimoto, S., Ikenaga, N., Jan van der Goot, A., & Sagis, L. M. C. (2025). Effects of screw configuration and interfacial properties on oil incorporation in high moisture extrusion. *Current Research in Food Science, 10*, Article 100989.

Heiden-Hecht, T., Wu, B., Schwärzer, K., Förster, S., Kohlbrecher, J., Holderer, O., & Frielinghaus, H. (2024). New insights into protein stabilized emulsions captured via neutron and X-ray scattering: An approach with β-lactoglobulin at triacylglyceride-oil/water interfaces. *Journal of Colloid and Interface Science, 655*, 319–326.

Ikenaga, N., Hashimoto, S., & Sagis, L. M. C. (2025). Effects of oil-water interfacial properties on protein structuring and droplet deformation in high moisture meat analogues containing oil. *Journal of Food Engineering, 387*, Article 112353.

Jafari, S. M., Doost, A. S., Nasrabadi, M. N., Boostani, S., & Van der Meeren, P. (2020). Phytoparticles for the stabilization of pickering emulsions in the formulation of novel food colloidal dispersions. *Trends in Food Science & Technology, 98*, 117–128.

Jeffries, C. M., Ilavsky, J., Martel, A., Hinrichs, S., Meyer, A., Pedersen, J. S., Sokolova, A. V., & Svergun, D. I. (2021). Small-angle X-ray and neutron scattering. *Nature Reviews Methods Primers, 1*(1), 70.

Kamani, K. M., Donley, G. J., Rao, R., Grillet, A. M., Roberts, C., Shetty, A., & Rogers, S. A. (2023). Understanding the transient large amplitude oscillatory shear behavior of yield stress fluids. *Journal of Rheology, 67*(2), 331–352.

Kornet, R., Yang, J., Venema, P., van der Linden, E., & Sagis, L. M. C. (2022). Optimizing pea protein fractionation to yield protein fractions with a high foaming and emulsifying capacity. *Food Hydrocolloids,, 126*, Article 107456.

Larson-Smith, K., Jackson, A., & Pozzo, D. C. (2010). Small angle scattering model for pickering emulsions and raspberry particles. *Journal of Colloid and Interface Science, 343*(1), 36–41.

Larson-Smith, K., Jackson, A., & Pozzo, D. C. (2012). SANS and SAXS analysis of charged nanoparticle adsorption at oil–water interfaces. *Langmuir, 28*(5), 2493–2501.

Li, M., He, Z., Li, G., Zeng, Q., Su, D., Zhang, J., Wang, Q., Yuan, Y., & He, S. (2019). The formation and characterization of antioxidant pickering emulsions: Effect of the interactions between gliadin and chitosan. *Food Hydrocolloids, 90*, 482–489.

Li, Z., Liu, W., Sun, C., Wei, X., Liu, S., & Jiang, Y. (2023). Gastrointestinal pH-sensitive pickering emulsions stabilized by zein nanoparticles coated with bioactive glycyrrhizic acid for improving oral bioaccessibility of curcumin. *ACS Applied Materials & Interfaces, 15*(11), 14678–14689.

Li, T., Senesi, A. J., & Lee, B. (2016). Small angle X-ray scattering for nanoparticle research. *Chemical Reviews, 116*(18), 11128–11180.

Liu, H., Yang, Y., Liu, Y., Cui, L., Fu, L., & Li, B. (2022). Various bioactive peptides in collagen hydrolysate from salmo salar skin and the combined inhibitory effects on atherosclerosis in vitro and in vivo. *Food Research International, 157*, Article 111281.

Nadendla, S. R., Rani, T. S., Vaikuntapu, P. R., Maddu, R. R., & Podile, A. R. (2018). Harpin encapsulation in chitosan nanoparticles for improved bioavailability and disease resistance in tomato. *Carbohydrate Polymers, 199*, 11–19.

Olakanmi, S., Karunakaran, C., & Jayas, D. (2023). Applications of X-ray micro-computed tomography and small-angle X-ray scattering techniques in food systems: A concise review. *Journal of Food Engineering, 342*, Article 111355.

Sabet, S., Rashidinejad, A., Melton, L. D., & McGillivray, D. J. (2021). Recent advances to improve curcumin oral bioavailability. *Trends in Food Science & Technology, 110*, 253–266.

Sagis, L. M. C., & Fischer, P. (2014). Nonlinear rheology of complex fluid–fluid interfaces. *Current Opinion in Colloid & Interface Science, 19*(6), 520–529.

Sagis, L. M. C., & Yang, J. (2022). Protein-stabilized interfaces in multiphase food: Comparing structure-function relations of plant-based and animal-based proteins. *Current Opinion in Food Science, 43*, 53–60.

Shah, U., Dwivedi, D., Hackett, M., Al-Salami, H., Utikar, R. P., Blanchard, C., Gani, A., Rowles, M. R., & Johnson, S. K. (2021). Physicochemical characterisation of kafirins extracted from sorghum grain and dried distillers grain with solubles related to their biomaterial functionality. *Scientific Reports, 11*(1), Article 15204.

Shen, P., Twilt, F., Deng, B., Peng, J., Schroen, K., Sagis, L. M. C., & Landman, J. (2025). Oil-water interface and emulsion stabilization by pulse proteins. *Food Hydrocolloids, 163*, Article 111093.

Tenorio-Garcia, E., Rappolt, M., Sadeghpour, A., Simone, E., & Sarkar, A. (2024). Fabrication and stability of dual pickering double emulsions stabilized with food-grade particles. *Food Hydrocolloids, 156*, Article 110327.

Tsabet, È., & Fradette, L. (2015). Effect of the properties of oil, particles, and water on the production of pickering emulsions. *Chemical Engineering Research and Design, 97*, 9–17.

Wang, L., Hu, Y., Yin, S., Yang, X., Lai, F., & Wang, S. (2015). Fabrication and characterization of antioxidant pickering emulsions stabilized by Zein/Chitosan complex particles (ZCPs). *Journal of Agricultural and Food Chemistry, 63*(9), 2514–2524.

Wang, L., Yin, S., Wu, L., Qi, J., Guo, J., & Yang, X. (2016). Fabrication and characterization of pickering emulsions and oil gels stabilized by highly charged zein/chitosan complex particles (ZCCPs). *Food Chemistry, 213*, 462–469.

Wen, J., Zhao, J., Jiang, L., & Sui, X. (2024). Oil-water interfacial behavior of zein-soy protein composite nanoparticles in high internal phase pickering emulsion. *Food Hydrocolloids, 149*, Article 109659.

Xiao, J., Li, C., & Huang, Q. (2015). Kafirin nanoparticle-stabilized pickering emulsions as oral delivery vehicles: Physicochemical stability and in vitro digestion profile. *Journal of Agricultural and Food Chemistry, 63*(47), 10263–10270.

Xiao, J., Wang, X.a., Gonzalez, A. J. P., & Huang, Q. (2016). Kafirin nanoparticles-stabilized pickering emulsions: Microstructure and rheological behavior. *Food Hydrocolloids, 54*, 30–39.

Yang, J., Shen, P., de Groot, A., Mocking-Bode, H. C. M., Nikiforidis, C. V., & Sagis, L. M. C. (2024). Oil-water interface and emulsion stabilising properties of rapeseed proteins napin and cruciferin studied by nonlinear surface rheology. *Journal of Colloid and Interface Science, 662*, 192–207.

Ye, Z., Landman, J., & Sagis, L. M. C. (2025). Kafirin-based pickering stabilizers: Tailoring interfacial properties with gum Arabic. *Food Hydrocolloids, 168*, Article 111530.

Ye, Z., Wang, Y., Shen, P., Sagis, L. M. C., & Landman, J. (2024). Effect of gum Arabic coating on release behavior of curcumin-loaded kafirin and zein composite nanoparticles. *Food Hydrocolloids, 156*, Article 110254.

Zhou, Z., Chen, M., Chen, Z., Wang, W., Cao, Y., & Xiao, J. (2024). Formation and properties of zein Particle-GMS Co-stabilized pickering emulsions: Insights into the complex interface. *Food Hydrocolloids, 149*, Article 109518.

Zhou, D., Xin, Y., Wu, B., Jiang, X., Wu, X., Hou, P., Qi, J., & Zhang, J. (2024a). Pickering emulsions stabilized by ternary complexes involving curcumin-modified zein and polysaccharides with different charge amounts for encapsulating β-carotene. *Food Chemistry, 433*, Article 137338.

Ikenaga, N., & Sagis, L. M. C. (2024). Interfacial moduli at large strains and stability of emulsions stabilised by plant proteins at high bulk shear rates. *Food Hydrocolloids, 146*, Article 109248.